ADVANCED HEALTHCARE MATERIALS
www.advhealthmat.de

Supramolecular Fibrous Hydrogel Augmentation of Uterosacral Ligament Suspension for Treatment of Pelvic Organ Prolapse

Beverly Miller, Wiley Wolfe, James L. Gentry, M. Gregory Grewal, Christopher B. Highley, Raffaella De Vita, Monique H. Vaughan, and Steven R. Caliari**

Uterosacral ligament suspension (USLS) is a common surgical treatment for pelvic organ prolapse (POP). However, the relatively high failure rate of up to 40% underscores a strong clinical need for complementary treatment strategies, such as biomaterial augmentation. Herein, the first hydrogel biomaterial augmentation of USLS in a recently established rat model is described using an injectable fibrous hydrogel composite. Supramolecularly-assembled hyaluronic acid (HA) hydrogel nanofibers encapsulated in a matrix metalloproteinase (MMP)-degradable HA hydrogel create an injectable scaffold showing excellent biocompatibility and hemocompatibility. The hydrogel can be successfully delivered and localized to the suture sites of the USLS procedure, where it gradually degrades over six weeks. In situ mechanical testing 24 weeks post-operative in the multiparous USLS rat model shows the ultimate load (load at failure) to be 1.70 ± 0.36 N for the intact uterosacral ligament (USL), 0.89 ± 0.28 N for the USLS repair, and 1.37 ± 0.31 N for the USLS + hydrogel (USLS+H) repair ($n = 8$). These results indicate that the hydrogel composite significantly improves load required for tissue failure compared to the standard USLS, even after the hydrogel degrades, and that this hydrogel-based approach can potentially reduce the high failure rate associated with USLS procedures.

1. Introduction

POP affects ≈50% of parous women[1] resulting in the descent of pelvic organs (vagina, bladder, uterus, small bowel, and rectum) due to weakened anatomical support structures.[2] In a healthy state, the pelvic floor organs are supported by the pelvic floor muscles, the uterosacral ligaments (USLs), and cardinal ligaments, which attach to the pelvis through connective tissue, while distal structures of the perineal body reinforce this supportive framework.[3,4] Due to the relatively high failure rate of some native tissue repairs, an estimated one-third of POP surgeries in 2010[5] relied on non-absorbable lightweight polypropylene (PP) mesh. However, unacceptable post-surgical complications, such as mesh erosion, exposure, contracture, and chronic pain, led the FDA to remove transvaginal mesh kits from the market in 2019.[6] While PP mesh is still used by many pelvic surgeons to perform sacrocolpopexies, the current international

B. Miller, M. G. Grewal, C. B. Highley, S. R. Caliari
Department of Chemical Engineering
University of Virginia
Charlottesville, VA 22903, USA
E-mail: caliari@virginia.edu
W. Wolfe
Scripps Institution of Oceanography
University of California
San Diego, La Jolla, CA 92 093, USA

The ORCID identification number(s) for the author(s) of this article can be found under https://doi.org/10.1002/adhm.202300086

DOI: 10.1002/adhm.202300086

J. L. Gentry, C. B. Highley, S. R. Caliari
Department of Biomedical Engineering
University of Virginia
Charlottesville, VA 22 903, USA
R. De Vita
Stretch Lab
Department of Biomedical Engineering and Mechanics
Virginia Tech
Blacksburg, VA 24 061, USA
M. H. Vaughan
Department of Obstetrics and Gynecology
University of Virginia
Charlottesville, VA 22 903, USA
E-mail: mv4w@hscmail.mcc.virginia.edu

climate and associated litigation surrounding the use of mesh leads many patients and their surgeons to seek mesh-free treatment options. The USLS procedure is a native tissue (suture only) alternative[7] to mesh augmentation, but it is plagued by a failure rate of up to 40%.[8,9] Therefore, there is an urgent clinical need to develop regenerative medicine strategies to provide safe and effective alternatives to mesh-based augmentation or suture only surgical procedures for POP. However, the development of treatment strategies for POP is hindered by the lack of funding for women's health research, the lack of information regarding the specific mechanisms of anatomical failure following USLS procedures, and lack of representative animal models.

Women's health is an important area of research that has been chronically underfunded and understudied.[10] For centuries the male body was the default for medical research and advancement due to the misconception that women's menstrual cycles would confound results. Increasing recognition of the unique aspects specific to women's health[11] has likely been influenced by the National Institutes of Health revised guidelines.[12] The 1994 update required women be included in all NIH-funded clinical studies while the 2016 revision extended the "sex as a biological variable" requirement to animal studies. To address the substantial gaps in medical knowledge, researchers have leveraged tissue engineering approaches to transform our understanding of ovarian follicle development,[13,14] endometriosis,[15] gynecological cancers,[16] and other disorders of the endometrium.[17] In addition, special journal issues focusing on engineering for women's health[18–20] and in-depth review articles[21,22] have increased visibility for this body of work. However, improving the quality of women's health research cannot be done without increasing government funding for female-specific disorders or developing research methods that are specifically designed for women.[23] By investing in research and innovation in women's health, we can improve the quality of care and outcomes for female-specific disorders such as POP.

According to recent studies,[24] a woman's current lifetime risk of undergoing prolapse surgery is ≈20%,[24] and that number is expected to rise in the coming years as the population ages. Additionally, the high failure rate of the USLS procedure results in up to a 33% reoperation rate to correct the recurrent prolapse.[25] Nevertheless, the specific mechanisms of anatomical failure following USLS are not well understood. Surgical repair of POP via the USLS procedure utilizes the dense collagenous sacral region of the USL to restore the vagina and surrounding structures to their anatomical positions in the abdominal compartment via absorbable or non-absorbable sutures. In a recent study, Bowen and colleagues showed that the primary mechanism of failure after USLS is apical descent, with anterior vaginal wall lengthening, inferior displacement of the perineal body, shortening of the posterior wall, and increased introitus size with strain being secondary factors associated with failure.[26] However, data examining the specific mechanism of apical descent failed to identify whether the apical descent was caused by suture failure, lengthening or insufficiency of the ligaments themselves, inappropriate healing of the vaginal/suture/ligament interface, or demographic factors such as obesity, age, and hormonal status. It is likely that the true mechanism of failure is multifactorial and involves many of these components together. In this study, we hypothesize that the primary mechanism of failure involves inappropriate healing of the vaginal-ligament interface, leading to a lack of mechanical stability of the anatomical connections. With the demand for surgical treatment of POP predicted to increase by nearly 50% by 2050,[27] there is an urgent clinical need to develop regenerative medicine and tissue engineering strategies to provide safe and effective alternatives to the current standard of care.

Within the tissue engineering community, there is growing interest in synthetic or biological materials to augment native tissue repairs.[28,29] Namely, biodegradable scaffolds made from decellularized matrices or polymers engineered to interact with the host tissue to promote constructive remodeling and integration[30–33] could be promising therapeutic platforms for prolapse repair, and may address several potential mechanisms of prolapse recurrence. Hydrogel biomaterials specifically provide an attractive alternative to mesh-based treatments due to the variety of material systems and chemistries available that can be tailored to the pelvic floor microenvironment. The ideal biomaterial for use in pelvic floor reconstructive surgeries is yet to be determined,[34] but refinement of animal models can assist in the development of new materials. Several animal models including rats, mice, rabbits, sheep, swine, and non-human primates have been utilized[35] in the study of pelvic organ prolapse with rodent models being optimal due to low cost and general accessibility. Despite this, the first POP surgical treatment rodent model was only recently established by our team.[36] Previous studies investigating materials for prolapse repair in rats have used an abdominal hernia repair model[37–42] due to the convenience of the established animal model[43,44] and perceived conservation of outcomes between the abdominal wall and the pelvic floor.[45,46] Conversely, while abdominal wall studies have demonstrated beneficial outcomes using increasingly stiff constructs,[29,47] pelvic floor studies have found that increased stiffness is directly linked to the deterioration of vaginal smooth muscle and the surrounding pelvic floor.[40,48] This "stress-shielding" phenomenon has also been seen in studies of bone[49] as well as tendons and ligaments,[50] where the stiffer material shields the adjacent tissue from experiencing physiological loads,[51] causing the less stiff tissue to degenerate.[34] Given this information, the abdominal wall hernia repair procedure is not the proven "proof of concept" model[45,52] that it was once thought to be. This again highlights the importance of developing research methods tailored to female anatomy and biomaterials that consider female tissue structures.

In this work, we present what we believe is the first study to use a rodent prolapse model to investigate a hydrogel biomaterial for the treatment of POP. To address the need for alternative materials and a suitable animal model to investigate prolapse repair, our lab developed a hyaluronic acid (HA) based fibrous hydrogel[53] as well as a rodent USLS model[36] to investigate the augmentation of native tissue repair procedures. A multiparous rat model was used due to its cost-effective nature and literature demonstrating the similar USL anatomy, cellularity, and matrix composition between rodents and humans.[54] Additionally, since failure of the native tissue repair is not well understood, the strength of the USL structures were assessed in situ with their anatomical connections left intact to provide mechanical data about the role the USL plays in USLS suspension. The central aim of this study was to determine the impact of augmenting the USLS procedure with a degradable hydrogel on the mechanical stability

of the vaginal-ligament interface. Our hypothesis was that the hydrogel augmentation of USLS would improve tissue integration at the USL-vaginal vault junction, therefore improving stability of the repair compared to sutures alone. Using a mechanical pull-off test,[55] procedures that included the hydrogel augmentation demonstrated a significant increase in force required for failure compared to the USLS repair alone. Additionally, we report relative collagen and muscle fiber content for the experimental groups, showing that hydrogel augmentation supports collagen and muscle levels more similar to the native USL than USLS alone. The findings of this research not only demonstrate the potential of hydrogel biomaterials to augment the treatment of POP, but also offer new mechanical and histological data for the rodent pelvic floor following USLS surgery.

2. Results and Discussion

This study presents the experimental outcomes following investigation of a hydrogel biomaterial for augmentation of the uterosacral ligament suspension (USLS) procedure in rats. We utilized our lab's recently developed USLS rodent model[36] and supramolecularly-assembled injectable and photocurable fibrous hydrogel[53] as a potential therapeutic for the treatment of POP. This is significant since there is an urgent clinical need for materials intended for the treatment of prolapse to be tested in pelvic floor models. While the mechanisms of mesh adverse events are not fully understood,[48] it has become clear that the planes of fat, muscle, and fascia of the abdominal hernia repair rat model[46] do not properly represent the smooth muscle and mucosa of the vagina and surrounding pelvic floor structures. Moreover, in addition to the USLS augmentation being more relevant for the investigation of potential prolapse therapeutics, previous work has demonstrated several similarities between rat and human USLs,[54] further demonstrating the benefits of the rodent model. The rodent model also allows researchers to control several variables, such as parity, which we controlled for in this study. To the authors' knowledge, this is the first study to investigate the use of a hydrogel biomaterial for augmentation of the USLS procedure.

2.1. Preparation of the Injectable and Fibrous Hydrogel

2.1.1. Fabrication of the Guest–Host Assembled Hyaluronic Acid Hydrogel Fibers

Of the many classes of materials that have been used in tissue engineering, hydrogels have emerged as one of the most prominent and versatile as they can provide a hydrated 3D environment that mimics many native soft tissue properties.[56] Polymeric hydrogels are especially attractive biomaterial platforms due to their tunable mechanical properties and ease of processing.[57,58] Since mesh-based augmentation is associated with vaginal tissue degeneration,[48,59] there is an urgent clinical need for materials that can mimic mechanical properties of the pelvic floor tissues. We chose hyaluronic acid (HA) as our therapeutic biomaterial platform due to its hydrophilicity, degradability in vivo, and its role in supporting tissue repair.[60] Here, the guest-host assembled hyaluronic acid (HA) hydrogel nanofibers were encapsulated in a matrix metalloproteinase (MMP)-degradable HA hydrogel, creating a fiber-hydrogel composite that was delivered to the suture sites of the USLS procedure (**Figure 1**). The guest (adamantane, Ad) and host (β-cyclodextrin, CD) modified fiber system leverages supramolecular chemistry that both enables facile injection for minimally invasive delivery and stabilizes the hydrogel post-injection. Both guest and host hydrogel fibers included photocross-linkable methacrylate groups that were utilized for stabilizing the fiber structure following electrospinning. In addition to the photocross-linking of the hydrogel fibers following electrospinning, the final fiber-hydrogel composite was also photocross-linked after injection at the suture site (Figure S1, Supporting Information). When the hydrogel fibers are mixed, the guest and host groups interact via hydrophobic non-covalent associations, creating a solid hydrogel until shear forces during injection disrupt the non-covalent interactions to create a "liquid-like" state. In Figure 1C, delivery of the hydrogel following hysterectomy is schematically shown where the hydrogel is applied over the sutures and surrounding tissue of the USL-vaginal vault created during the USLS procedure. For added stabilization of the self-assembling fibers within the abdominal cavity, the guest and host fibers were encapsulated in methacrylated peptide-modified HA (MePHA) engineered to be MMP-degradable, which allowed for secondary cross-linking via UV light.

2.1.2. Mechanical Characterization and Cross-Linking of the Injectable Fibrous Hydrogel

HA is an advantageous polymer choice in hydrogel design because it can be modified with reactive cross-linking groups to enable control of material biophysical properties (i.e., stiffness) and electrospun to create extracellular matrix (ECM)-like nanofibers mimicking native tissue.[61–63] However, replicating host tissue properties following prolapse surgery is challenging due to the limited literature on biomechanical properties. Studies done on the human prolapsed vagina report viscoelastic mechanical properties[64] and an elastic modulus range of 2 – 13 MPa.[65] The few studies that have investigated rodent pelvic support fixed the entire pelvic region and reported a linear stiffness of $\approx$3 N mm^{-1} for parous rats.[66,67] To our knowledge, there have been no experimental studies conducted on the mechanics of the pelvic floor tissues following surgical treatment of POP, likely due to lack of available tissue samples and lack of prolapse repair animal models. Ideally, the hydrogel augmentation should enhance the properties of the structurally impaired vaginal tissue. Therefore, this study utilized our lab's recently developed fibrous hydrogel platform[53] to better understand the ideal biomaterial design for augmenting prolapse repair. Oscillatory shear rheology (**Figure 2**) confirmed the hydrogel had robust mechanical properties under low strain conditions and underwent reverse gelation at higher strains mimicking injection prior to UV cross-linking. This is shown via a storage modulus that is higher than the loss modulus of 3.85 $\pm$ 0.61 kPa versus 0.65 $\pm$ 0.11 kPa respectively in conditions of low strain and a storage modulus that is lower than the loss modulus of 0.17 $\pm$ 0.01 kPa versus 0.53 $\pm$ 0.03 kPa respectively (n = 3). Importantly, the hydrogels showed full recovery of their viscoelastic properties after cyclic straining (Figure 2A). Once UV light was applied to the material, the storage modulus rapidly increased to 4.91 $\pm$ 0.51 kPa, demonstrating the

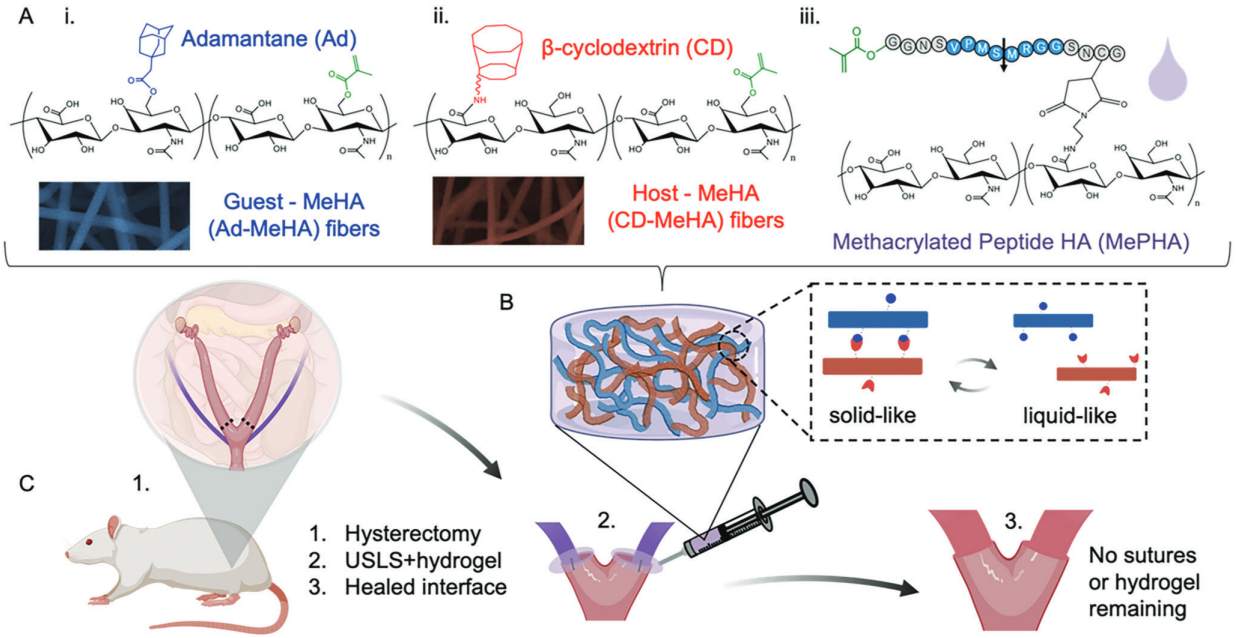

Figure 1. Schematic presentation of the composition of the fibrous injectable hydrogel system and uterosacral ligament suspension (USLS) augmentation process. A) Hyaluronic acid (HA) was modified with either i) the guest (adamantane, Ad) or ii) host (β-cyclodextrin, CD) molecules to create guest and host hydrogel fibers. Both guest- and host-modified HA also contained methacrylate groups to enable fiber stabilization via photocross-linking after electrospinning. Separately, HA was functionalized with iii) a matrix metalloproteinase (MMP)-degradable photocross-linkable peptide for encapsulating the fibers to produce B) a "solid-like" composite hydrogel capable of shear-thinning for injectable delivery to C) the sutures of the USLS procedure following hysterectomy. In situ photocross-linking produced a mechanically stabilized biomaterial (shear modulus ≈4 kPa) that was fully degraded, as were the sutures, by the end of the study (24 weeks post-operative). Schematics created with BioRender.com.

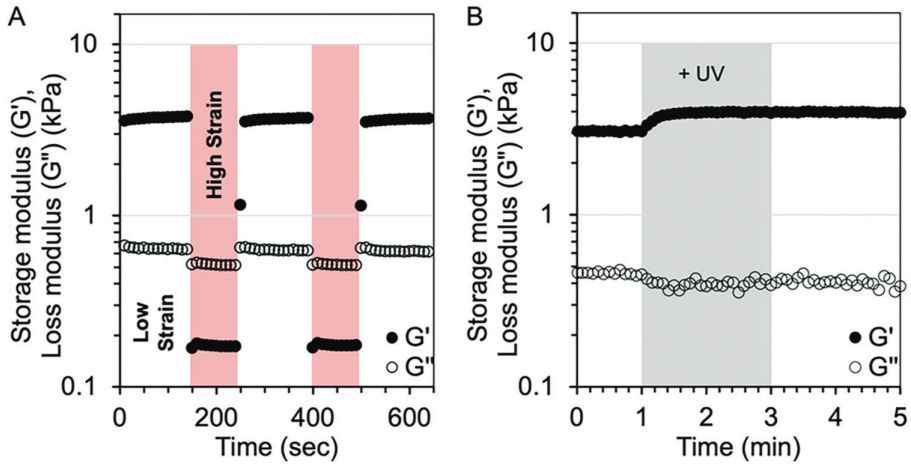

Figure 2. The mechanical properties of the fibrous hydrogel were measured using oscillatory shear rheology, showing A) a five-step strain sweep of low strain (0.5%, 100 s) and high strain (250%, 100 s) to illustrate the shear-thinning and self-healing properties of the hydrogel. Guest-host interactions between the fibers produced a solid-like material shown by the higher storage moduli than storage moduli at low strain. With the liquid-like behavior at high strain, shown by the storage moduli being lower than loss moduli, the material demonstrated shear-thinning and self-healing properties. B) In the presence of LAP photoinitiator, 2 min of UV light exposure (365 nm, 10 mW cm^{-2}) increased the storage modulus of the material, indicating the cross-linking of the free methacrylates of the encapsulating MePHA hydrogel. All tests were performed at 37 °C, $n = 3$.

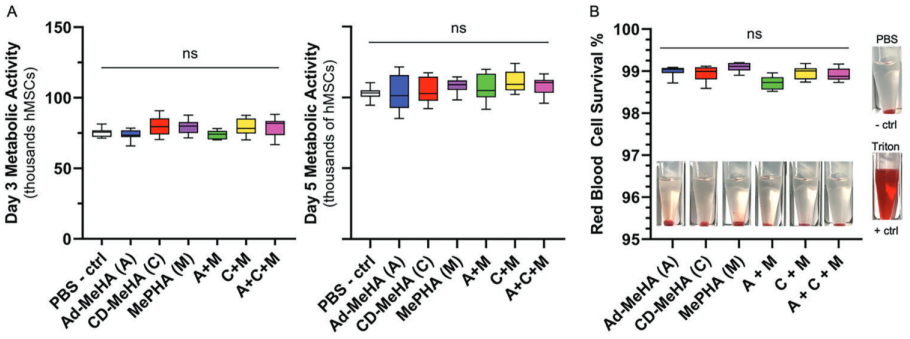

Figure 3. In vitro cytocompatibility and hemocompatibility tests. A) Metabolic activity, measured via an Alamar blue assay, of human mesenchymal stromal cells (hMSCs) after 3 (*left*) and 5 (*right*) days of culture. Cells were seeded at 30000 cells per well. hMSC culture was performed in the presence of hydrogel components, while cells cultured in the presence of PBS were used as the negative control. Number of cells were calculated using a standard curve created at the time of cell seeding. $n = 4$. B) Percentage of rat red blood cell (RBC) survival following incubation with hydrogel components, PBS (neg control), and Triton-X100 (pos control). $n = 4$. *ns* represents no statistically significant differences between experimental groups. The data were statistically analyzed by one-way ANOVA followed by Tukey-Kramer multiple comparisons testing.

Table 1. Values from in vitro biocompatibility tests with mean ± standard deviation. A) Cytocompatibility values reported as thousands of cells ($n = 4$) and B) Hemocompatibility values reported as percentage red blood cell (RBC) survival, calculated using Equation (1) (see Experimental Section). ($n = 4$).

A) Cytocompatibility (thousands of cells)			B) Hemocompatibility (% RBC survival)	
	Day 3	Day 5		
PBS – ctrl	75.2 ± 2.9	102.8 ± 4.0		
Ad-MeHA (A)	74.0 ± 3.4	103.2 ± 12.2	Ad-MeHA (A)	99.0 ± 0.1%
CD-MeHA (C)	79.8 ± 6.5	105.4 ± 9.0	CD-MeHA (C)	98.9 ± 0.2%
MePHA (M)	79.2 ± 5.1	112.7 ± 5.7	MePHA (M)	99.1 ± 0.1%
A+M	74.0 ± 2.9	107.1 ± 9.7	A+M	98.7 ± 0.2%
C+M	79.3 ± 5.7	110.7 ± 7.4	C+M	99.0 ± 0.2%
A+C+M	79.7 ± 6.3	108.7 ± 6.0	A+C+M	98.9 ± 0.2%

stabilization of the hydrogel that would form over the suture tissue interface for the USLS augmentation (Figure 2B). Crosslinking was carried out with 365 nm light at an intensity of 10 mW cm^{-2} for 2 min.

2.2. In Vitro Biocompatibility

Hydrogels formed from natural materials such as HA offer inherent biocompatibility, making them ideal candidates for tissue engineering applications.[60,68] Nevertheless, it is crucial to demonstrate in vitro biocompatibility of any developed material system before proceeding with in vivo studies. As such, we conducted cytotoxicity and hemocompatibility assays to evaluate the biocompatibility of our fibrous hydrogel composite.

2.2.1. Cytocompatibility

Figure 3 shows the cytotoxicity of each hydrogel component (Ad-MeHA(A), CD-MeHA(C), and MePHA(M)) and hydrogel composite mixture when exposed to human mesenchymal stromal cells (hMSCs) in culture. Cytotoxicity results are summarized in **Table 1**A. hMSCs were chosen for this evaluation because of their multipotent differentiation capacity, which allows them to differentiate into various cell types, including smooth muscle cells and fibroblasts, that are relevant to pelvic floor tissue regeneration. The cytocompatibility evaluation was also performed on mouse myoblast C2C12 cells to demonstrate broader biocompatibility (Figure S2 and Table S1, Supporting Information). No statistically significant differences were observed in cell metabolic activity between the polymer groups and the control group incubated in media with PBS after 3 and 5 days of culture. These cytocompatibility results align with previous findings using the fibrous hydrogel system, where hMSC viability remained above 85% following injection and after 7 days of culture.[53]

2.2.2. Hemocompatibility

Materials implanted in vivo will encounter the surrounding tissue as well as bodily fluids, such as blood. Assays that investigate how red blood cells (RBCs) react with the scaffold provide useful information about possible consequences of biomaterial-blood interactions.[69] While the fibrous hydrogel is designed to mimic the native ECM and support tissue function, interactions between the biomaterial and blood were evaluated prior to implantation. Figure 3B shows the hemocompatibility results for

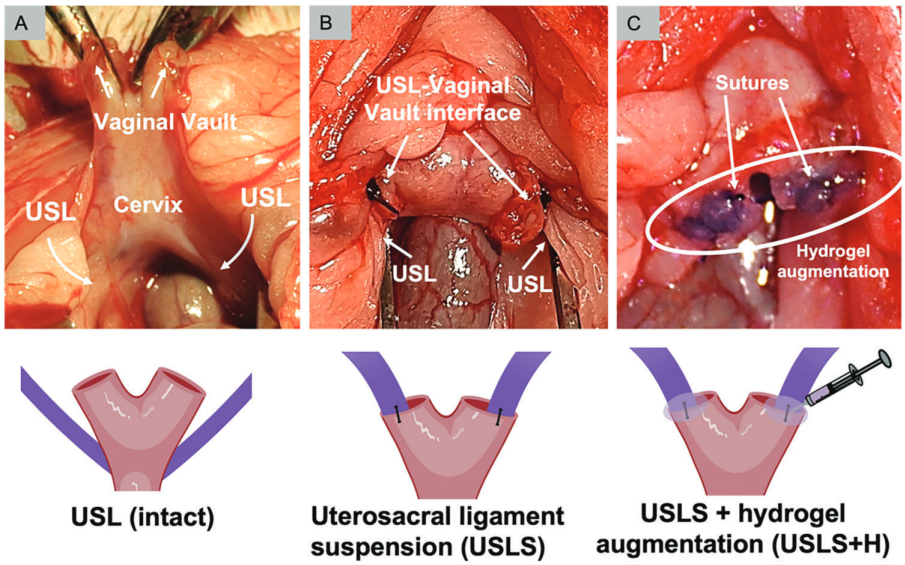

Figure 4. Schematic presentation of the uterosacral ligament suspension (USLS) surgical process and hydrogel augmentation (USLS+H). A) Removal of the uterine horns creates the vaginal vault structures with the USLs seen directly adjacent to the cervix. B) The USLS procedure secures the vaginal vault high on the USLs via a single suture such that the vaginal vault is elevated toward the sacrum. C) For hydrogel augmentation, 20 µL of hydrogel per side was administered such that the suture at the USL-vaginal vault interface was completely covered prior to 2 min of UV cross-linking (365 nm) to further stabilize the hydrogel. Schematics created with BioRender.com.

each component using freshly collected rodent RBCs. Values for each group are summarized in Table 1B. After incubation with the material components, the RBCs showed no obvious hemolysis when compared to the Triton-X100 group (positive control). The low hemolysis ratio indicates that the fibrous hydrogel scaffold possesses satisfactory blood compatibility. Together, these in vitro experiments demonstrated biocompatibility of the fibrous hydrogel composite.

2.3. Augmentation of Rodent USLS

The overall body of tissue engineering literature for prolapse repair is dominated by mesh-based augmentation, with the implication that native tissue and mesh-based repairs are of the few suitable treatment options for POP. With this narrow focus on mesh-based therapeutics, it is unsurprising that the search for ideal tissue remodeling materials for urogynecological repair is ongoing. A lack of accessible, and surgically accurate, animal models is at least partially to blame for the lack of non-mesh biomaterial investigation. In fact, just last year Bickhaus and colleagues were the first to use a rodent model to investigate a new polycarbonate urethane mesh for pelvic reconstruction via implantation in the vagina.[70] However, this study still focused on a mesh construct and used a surgical method not used in humans when repairing prolapse. By contrast, our rodent USLS procedure mimics the surgical method used in humans, establishing this work as the first study to investigate biomaterial hydrogel augmentation for prolapse repair in a surgically accurate rodent model.

In this study, we aimed to investigate the efficacy of our fibrous hydrogel composite using our established rat USLS surgery model.[36] All animals were maintained and treated under the approval of the University of Virginia Institutional Animal Care and Use Committee. All rats were multiparous, meaning that they had delivered prior litters (two in our study). Thirty Lewis rats (Charles River Laboratories) between 4 and 6 months of age were used to accommodate the two-litter requirement. Detailed surgical instructions with reproducible steps are published elsewhere.[36] Briefly, following anesthetization using isoflurane and aseptic preparation of the surgical site, a vertical midline skin incision was made down the linea alba and the muscle layer underneath. Removal of the uterine horns (hysterectomy) created the vaginal vault structure with the intact USLs directly below (**Figure 4**A). Ovaries were left in situ. The USL-vaginal vault interface was created by suturing the remaining vaginal vault tissue to the USLs (Figure 4B). Animals were randomly assigned to one of the following experimental groups: sham surgery with no prolapse repair (USL; $n = 8$), prolapse repair (USLS; $n = 8$), or prolapse repair with hydrogel augmentation (USLS+H; $n = 8$).

For the animals randomly assigned to the USLS+H experimental group, the injectable fibrous hydrogel was administered and then UV cross-linked to stabilize the material over the suture (Figure 4C). Prior to delivery, the fibrous hydrogel composite was prepared using sterile technique. Each component (Ad-MeHA fibers, CD-MeHA fibers, MePHA) was sterilized by overnight lyophilization followed by germicidal UV irradiation for 2–3 h. Additionally, the LAP photoinitiator stock solution was sterile filtered before use. The supramolecular nature of the guest-host fibers kept the 20 µL of hydrogel delivered to each suture site, total of 40 µL per animal, localized while the UV cross-linking further stabilized the material. We chose UV photopolymerization for in situ stabilization as it is a commonly used technique for covalent cross-linking of hydrogels.[71–73] Hydrogel delivery and

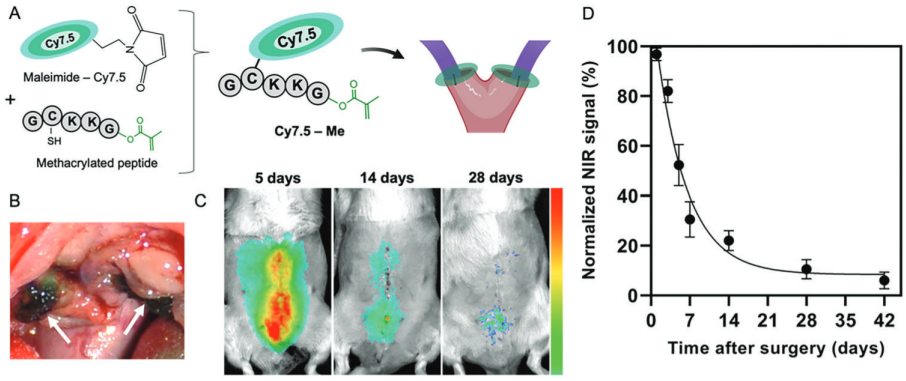

Figure 5. In vivo fibrous hydrogel degradation. A) Methacrylated peptide conjugated with sulfo-maleimide cyanine 7.5 (Cy7.5-Me). The methacrylated peptide was first synthesized via solid-phase synthesis and then the Cy7.5 was tethered via maleimide-thiol click chemistry. The methacrylate on the peptide allowed for covalent conjugation of the Cy7.5 dye to the HA backbone via photocuring before scaffold formation. B) Arrows point toward the Cy7.5-labeled hydrogel following delivery. Erosion of the fibrous hydrogel, as represented by the C) serial in vivo optical images, was D) quantified by Cy7.5 signal decay ($n = 4$) showing an exponential one-phase decay ($R^2 = 0.953$).

suture site UV stabilization is depicted in Figure S1C (Supporting Information). However, to utilize the minimally invasive capabilities of the fibrous hydrogel in another animal model or in human treatment, alternative in situ stabilization mechanisms such as redox-initiated polymerization would potentially need to be explored. Delivery of the hydrogel was not minimally invasive in this study, but the benefit of the self-healing property of the material cannot be overstated. The syringe and needle delivery allowed for precise placement and minimized migration of the material prior to UV stabilization. Material migration is a known issue when implanting biomaterials in vivo.[56] Given the exposure of the implanted material to the abdominal cavity, the USLS model is no different. Further, while the injectability was used to augment the suture site in a "wound dressing" manner, the injectable delivery could allow for tissue bulking in addition to augmentation in future studies. With these concepts in mind, other self-healing biomaterials may be good candidates for prolapse repair due to the benefits of localized and minimally invasive delivery.

2.4. In Vivo Assessment of Hydrogel Degradation

In developing materials for pelvic floor applications, biodegradability has been identified as a key consideration.[28,40] In vivo erosion of the fibrous hydrogel scaffold was investigated by covalently attaching a near-infrared (NIR) dye to the supramolecular hydrogel fibers and monitoring the corresponding loss in signal intensity over a 6 week period (**Figure 5**). In addition, the results from the fluorescent imaging confirmed sustained placement of the hydrogel at the suture sites. A maleimide-modified cyanine 7.5 fluorophore (Cy7.5, Lumiprobe Corporation, Figure S3, Supporting Information) was conjugated to a methacrylated peptide (Figure S4, Supporting Information) to enable UV light-mediated methacrylate cross-links to covalently attach the Cy7.5-labeled methacrylated peptide (Cy7.5-Me, Figure S5, Supporting Information) to the hydrogel material. In Figure 5B the labeled hydrogel covers the sutures of the USLS procedure with Figure 5C showing serial in vivo optical images. The fibrous injectable hydrogel scaffold demonstrated faster erosion over the first week (losing >50% of the NIR signal) and ≈95% degradation after six weeks, showing an exponential (one-phase) decay erosion trend as shown in Figure 5D. The rapid degradation is hypothesized to be due to the small amount of material, the exposure to abdominal movements (physical) and fluid erosion (convective fluid movement), and cell-mediated enzymatic degradation. It is unclear if this degradation rate is ideal as there is a limited understanding of the remodeling rate at the USL-vaginal vault junction. General tendon and ligamental remodeling has a known timescale of a few weeks,[74] but that does not necessarily represent the supportive ligaments of the pelvic floor. Additionally, there is no set time-scale reported for vaginal and pelvic smooth muscle remodeling, but there are clear examples of hormone[75,76] and strain dependence.[77] While only a semi-quantitative assessment of degradation, these results demonstrate the degradability of the fibrous HA composite scaffold and provide context for future studies investigating biomaterial degradation in POP models.

2.5. In Situ Assessment of Specimen Mechanical Integrity 24 Weeks Post-Operative

While urogynecological research is still in its infancy compared to other fields, this work builds on previous work[65,78] attempting to provide biomechanical context for pelvic floor tissues. At 24 weeks post-operative, the mechanical properties of the USL-vaginal vault interface after suture only (USLS) and hydrogel augmentation (USLS+H) procedures were assessed and compared with mechanical properties of the intact the USL (**Figure 6**). Mechanical "pull-off" tests were performed in situ (Instron, 10 N load cell, 0.00025 N resolution). Specimens were preloaded at 0.15 N and then preconditioned at an elongation rate of 0.1 mm s^{-1} as described in our previous work.[36] Data points were collected every 0.1 s and analyzed via MatLab. The sutures or the sutures + hydrogel were completely resorbed at the time of testing. Briefly, the USL-vaginal vault interface of the USLS and the USLS with hydrogel (USLS+H) groups were exposed

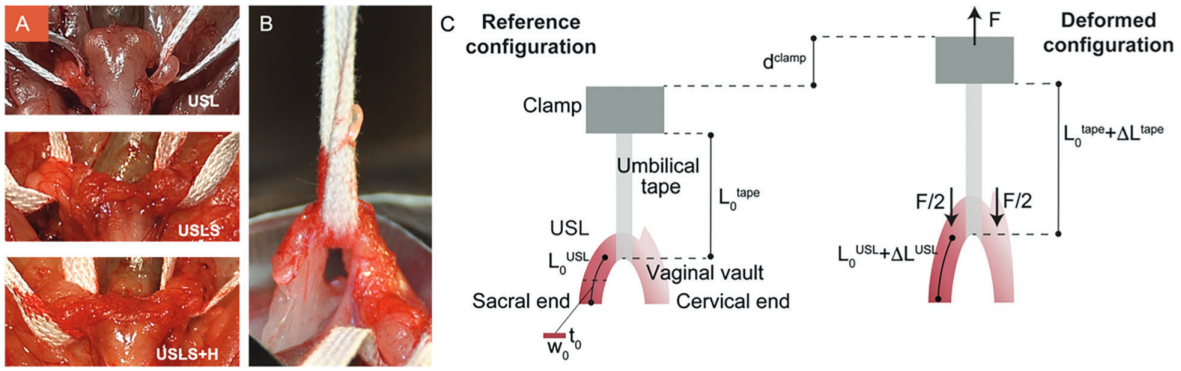

Figure 6. In situ tensile tests pulled to failure. A) Tissue preparation for tensile testing where the umbilical tape was placed underneath the cervical end of the structure. B) Sample undergoing the "pull-out" test to failure with a schematic detailing the measurements in C) the reference configuration and the deformed configuration.

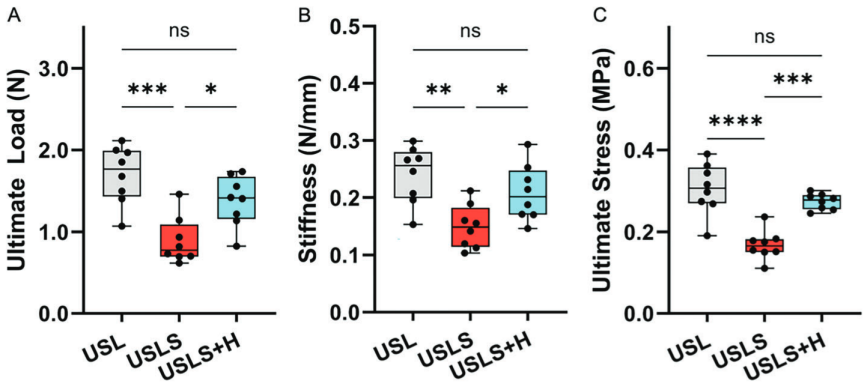

Figure 7. Analysis of sample mechanical properties based on the load-displacement data and calculated stress. Data presented are A) force at failure, or ultimate load, B) slopes of the load-displacement curves, C) and the stress at failure, or ultimate stress. $n = 8$, *ns* represents no statistically significant difference, * $P < 0.05$, ** $P < 0.01$, *** $P < 0.001$, **** $P < 0.0001$. The groups are as follows: USL, intact uterosacral ligament; USLS, suture only surgical repair; USLS+H, hydrogel augmentation of the USLS surgical repair. The data were statistically analyzed by one-way ANOVA followed by Tukey-Kramer multiple comparisons testing.

such that umbilical tape could be placed beneath the structure and then clamped in the tensile tester grip. For the intact tissue comparison, the umbilical tape was placed beneath the intact USL structure. A total of 8 specimens ($n = 8$) are reported per group. After specimen preparation, samples were tested until failure where Figure 6B shows a sample mid-test and Figure 6C is an overview of defined parameters of the testing. Due to the nature of comparing intact tissue (USL) to surgically altered tissue (USLS and USLS+H), the failure location differed between samples. For the specimens that underwent the USLS surgical procedure, failure occurred at the sutured interface. In contrast, the failure for intact specimens occurred roughly midline along the USL.

Load-displacement curves are reported in Figure S6 (Supporting Information) where displacement is defined as $d^{clamp} - \Delta L^{tape}$, where d^{clamp} is the displacement of the clamp (or cross-head displacement) and ΔL^{tape} is the change in length of the umbilical tape. The presence of several peaks in the load as the displacement increased demonstrated that the failure of the USLs, or the surgically repaired tissue, occurred gradually. As is typical for soft tissues, data were characterized by an initial toe region, a more linear region, and then a nonlinear failure region where the gradual failure is likely due to bundles of tissue fibers breaking at various load levels.

2.5.1. Mechanical Pull Off Testing Analysis

Results showed an ultimate load of 1.70 ± 0.36 N for the intact uterosacral ligament (USL), 0.89 ± 0.28 N for the USLS repair, and 1.37 ± 0.31 N for the USLS+H group (**Figure 7**). The stiffness, defined as the steepest positive slope measured over a 1 mm elongation interval, was 0.48 ± 0.10 N mm^{-1} for the intact USL, 0.28 ± 0.07 N mm^{-1} for the USLS procedure, and 0.42 ± 0.10 N mm^{-1} for the USLS+H group. Stress data were computed under the assumption that the USL was loaded along one axis as shown in Figure 6C. Next, the ultimate stresses were calculated using the ultimate load data. Tissue measurements including the thickness (t_0), width (w_0), and gauge length (L_0^{USL}), where the gauge length was defined as the length of the USL from the sacral attachment to the vaginal vault/cervical insertion, were also obtained (Figure 6C). Average cross sectional thickness

Table 2. Values from sample mechanical properties based on the load-displacement data and calculated stress with mean ± SEM. ($n = 8$). The groups are as follows: USL, intact uterosacral ligament; USLS, suture only surgical repair; USLS+H, hydrogel augmentation of the USLS surgical repair.

	Ultimate Load [N]	Stiffness [N/mm]	Ultimate Stress [kPa]
USL	1.70 ± 0.36	0.48 ± 0.10	0.30 ± 0.06
USLS	0.89 ± 0.28	0.28 ± 0.07	0.17 ± 0.04
USLS+H	1.37 ± 0.31	0.42 ± 0.10	0.27 ± 0.02

and width were 1.9 ± 0.3 mm and 2.8 ± 0.2 mm while average gauge length was 12.3 ± 0.7 mm respectively. The ultimate stress in the tissue before complete failure was shown to be 0.30 ± 0.06 MPa for the intact USL, 0.17 ± 0.04 MPa for the USLS, and 0.27 ± 0.02 MPa for the USLS+H groups. Notably, for all mechanical testing data shown in Figure 7, hydrogel augmentation (USLS+H) resulted in statistically significant increases in mechanical properties compared to the USLS-only group. Additionally, there were no statistically significant differences in mechanical properties between the USLS+H and intact USL groups. All mechanical testing values are summarized in **Table 2**. These exciting results, obtained after the hydrogel and sutures were completely degraded, highlight the potential of this hydrogel therapeutic to promote long-term improvement in the mechanical stability of the USL-vaginal vault interface created in USLS procedures.

The mechanical testing protocol described here represents a new method to assess the entire USL and the additional support structures in situ rather than ex vivo, providing crucial mechanical data about the role the USL plays in USLS suspension. This testing methodology allowed us to test the weakest region of the USL, the cervical region, since the force was applied directly on this region through umbilical tape. During testing, the USL experienced not only tension, but inevitably also compression and shear given the geometry of the ligament and its position relative to the applied load. Moreover, to ensure that the USL was the primary anatomical structure being pulled, we secured the surrounding pelvic tissues to the base plate of the testing machine using a strong adhesive tape. Only the vaginal vault and USL structures were left exposed for testing. Although this prevented significant loading of other anatomical structures, other pelvic tissues were likely loaded and stretched together with the USL. The loads reported here may thus overestimate the loads that are experienced by the USL alone, without their connections to the pelvis. Despite these limitations, the load values we reported fall within the values reported in the literature when loading the rat vagina and USL attachments together in vivo[67] and uniaxially testing the isolated rat USL ex vivo.[79] The load-displacement curves are very similar to those reported by Donaldson and De Vita, both qualitatively and quantitatively.[79]

2.6. Histological Observation of Specimens 24 Weeks Post-Operative

To better understand the mechanism behind the hydrogel-mediated improvement in mechanical properties quantified in Figure 7, Masson's trichrome (MT) staining was used to visualize tissue specimens from the three experimental groups 24 weeks post-operative. **Figure 8** shows MT-stained representative images of whole tissue sections along with higher magnification images of the vaginal vault or vaginal vault-USL areas of interest. Collagen (*blue*) and muscle fibers (*red*) are visible in all groups with collagen bundles being the predominant visual feature of the intact vaginal vault (USL) group. Hematoxylin and eosin (H&E) staining was also performed to visualize tissue cellularity (Figure S7, Supporting Information).

2.6.1. Relative Collagen and Muscle Fiber Content of the USL-Vaginal Vault Interface

Collagen and muscle fiber quantification was performed in ImageJ (NIH) using the "RGB Measure" plugin (Figure S8, Supporting Information). With blue representing collagen and red representing muscle fibers, the tool measured the red and blue components of each pixel in each image. Percentages discussed here represent the average percentage of red and blue pixels measured per image per group. Compared to the USL control group (USL: 87.1 ± 0.7%), both the USLS and USLS+H groups demonstrated significantly lower relative collagen staining (USLS: 51.6 ± 0.7%, USLS+H: 72.4 ± 2.7%). However, the USLS+H group had significantly higher levels of collagen staining than the USLS group that were more similar to the USL group. Similarly, while significant differences were found between all groups in relative muscle fiber content (USL: 12.9 ± 0.7%, USLS: 48.4 ± 0.7%, USLS+H: 27.6 ± 2.7%), hydrogel augmentation promoted relative muscle fiber content that was closer to the USL group. In the intact USL specimens, muscle fibers make up the lining structures (cervical canal, veins) and along the distal edges of the vaginal vault where pelvic support ligaments attach. In the USLS and the USLS+H specimens, the muscle fibers are also evident in the lining areas but the muscle fiber content makes up more of the vaginal vault region than in the USL group, demonstrating the impact of the surgical intervention on the tissue. Results demonstrate the preservation of collagen for the group that experienced the hydrogel augmentation (USLS+H) compared to the collagen loss experienced by the group that experienced suture repair only (USLS). This suggests that the hydrogel augmentation may help prevent collagen loss following pelvic reconstructive surgery and could potentially lead to improved outcomes for women who undergo USLS surgery.

The MT stained tissue sections provide a visual representation of the distinct differences in tissue morphology between the three groups, with the USLS+H group being more similar to the intact USL group than the USLS suture-only group. Results here show the differences in collagen (*blue*) and muscle fiber (*red*) content where future studies could perform additional stains to delineate specific ECM protein components such as type I/III collagen (picrosirius red)[80] or elastin (Verhoeff–van Giesson, VVG).[81] Previous studies have predominantly reported composition for intact pelvic support tissues, reporting high collagen (70-80%) content and modest muscle fiber content (12-20%), similar to our findings of the intact vaginal vault.[54,81] However, the limited studies that have quantified collagen of the pelvic floor and vaginal structures following disruption of the pelvic support structures (i.e., prolapse) have reported a reduction in collagen in groups with

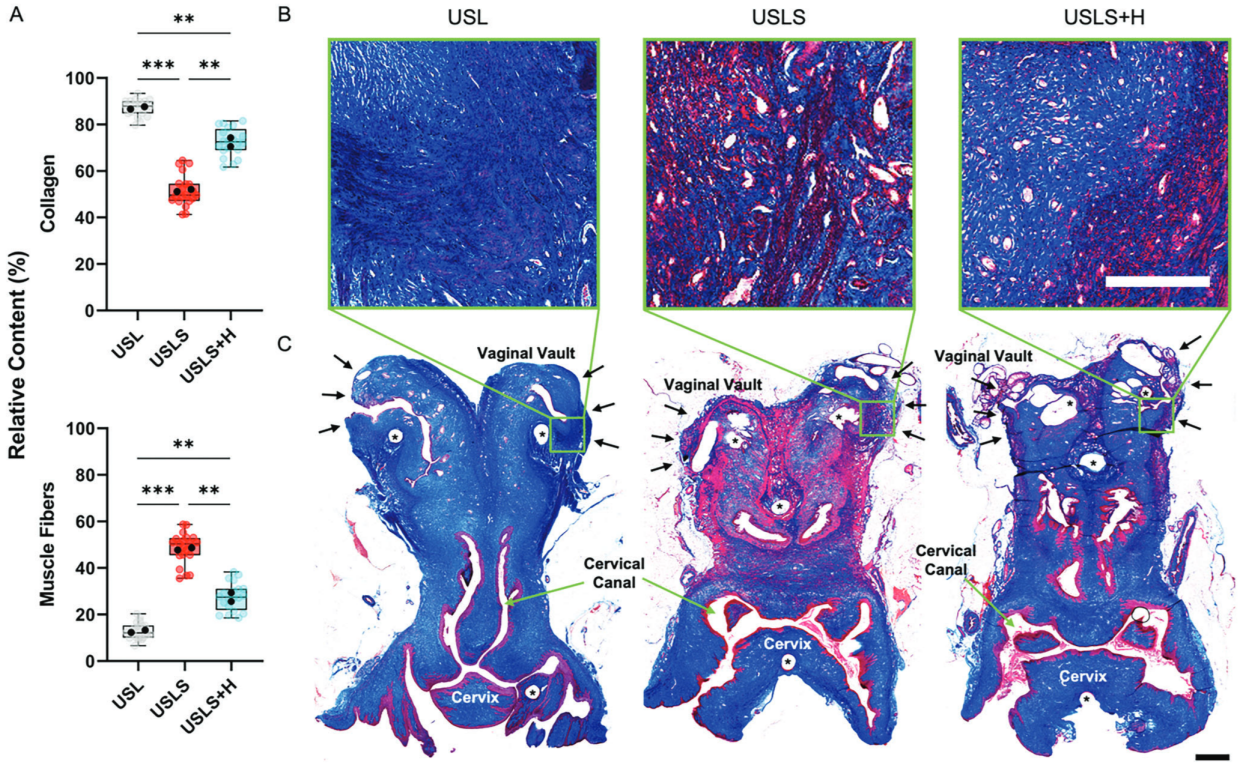

Figure 8. Masson's trichrome (MT)-stained female rat reproductive structures 24 weeks post-operative. A) Relative collagen (*blue*) and muscle fiber (*red*) contents of MT-stained USL, USLS, and USLS+H samples. Pixel color quantification performed via RGB measure tool in ImageJ (NIH). Colored and semi-transparent data points represent quantification of individual regions of interest (ROIs) from histology sections while the solid black data points represent the final averaged values for each animal, which were used for statistical analysis. $n = 2$ animals per experimental group, ** $P < 0.01$, *** $P < 0.001$. B) Representative images of the intact vaginal vault (USL group) and vaginal vault-USL sutured interface (USLS and USLS+H groups) post-operative used for relative color count percentage analysis (40x). Scale bar: 250 µm. C) Longitudinal sections of rat cervix and vaginal vault structures (10x). Black arrows indicate vaginal vault region of interest (USL group) or vaginal vault-USL interface region of interest (USLS and USLS+H groups). Scale bar: 1 mm. The asterisks mark the location of the pins placed when maintaining tissue orientation during formalin fixation. The data were statistically analyzed by one-way ANOVA followed by Tukey-Kramer multiple comparisons testing.

prolapse.[30,82,83] This, along with our findings that the USLS procedure was associated with decreased vaginal vault collagen content compared to the healthy control, suggests that pelvic reconstructive surgery may delay or permanently compromise healing and tissue remodeling within the pelvic structure ECM. With the hydrogel augmentation appearing to promote some recovery of collagen content and tissue remodeling capabilities in the USLS+H group, this work demonstrates the potential of hydrogel augmentation to improve outcomes of USLS surgery.

The fibrous hydrogel was chosen for this study due to its ability to mimic the fibrous microenvironment of the USL and pelvic support milieu. The effects of ECM-based bioscaffolds facilitating remodeling in damaged tissue have been well documented.[30,84] However, to our knowledge, this is the first paper to present histological data showing the benefits of hydrogel augmentation following USLS surgery in rodents. While the results of this study are exciting, it is important to acknowledge that this study uses animals with surgically-induced prolapse. Thus, if women with prolapse suffer from genetically deficient or inherently altered ability to promote healthy tissue growth, it is unlikely that the fibrous hydrogel would have the same effect. Nonetheless, we foresee the potential of the fibrous hydrogel to be applied to other uterine/vaginal/pelvic support surgeries.

2.7. Study Advantages and Limitations

The principal strength of this study was the use of a prolapse surgical model to investigate a potential therapeutic for prolapse repair. In the last year, the first study to describe implantation of a mesh biomaterial in the rodent vagina was published,[70] but moving away from mesh-based repairs is advantageous to explore a wider array of possible therapeutics. Other studies investigating materials for prolapse repair utilized abdominal wall hernia models which are poorly predictive of material compatibility with the pelvic organs.[46,48] Next, the in situ mechanical testing of the USL-vaginal interface following suture-only repair and repair with augmentation provides measurable outcomes to assess the therapeutic potential of the implanted material for POP. The mechanical testing protocol described here can also be adjusted for use in other pelvic floor models, expanding the range of tools available to researchers to measure outcomes of new biomaterial

interventions. Last, the surgical procedures were performed by one surgeon rather than multiple surgeons.

However, this study was subject to several limitations. Controlling for parity of the vendor available animals had the major drawback of receiving animals without exact age information. Without information regarding how recently the rats had delivered their second litters, it was not possible to control for animal weight. Additionally, the rodent pelvis has a horizontal orientation that does not replicate the gravitational effects seen in humans or non-human primates. This and the lack of spontaneous prolapse in the rat models does limit some applicability of these results to humans, but the use of multiparous rats is a strength of this work since this accounts for the leading risk factor in the development of POP.[85] Next, regarding the histological analysis, the *n* of 2 animals is insufficient to make strong claims regarding changes in tissue composition and morphology, but statistical trends were still quantified in these data. Future work will look at short-term time points as well as long-term data collection to better understand the role of the hydrogel during acute post-surgical healing. An increased sample size will also help to strengthen any future claims. Last, although it is ideal to have a study with a single surgeon, the homogeneity in surgical technique does not capture the variability in outcomes from a diverse population of surgeons.[86]

3. Conclusion

With this study we describe the first hydrogel augmentation of USLS in rodents, demonstrating the usefulness of the USLS rat model in the investigation of therapeutics for prolapse treatment. With a reoperation rate following prolapse surgery of up to 30%[27,87,88] and major drawbacks to the use of mesh-based biomaterials, there is an urgent need explore alternative biomaterials with properties that are more compatible with the vagina and pelvic floor. The USLS model provides the means for these materials investigations. We were able to assess the in vivo efficacy of our supramolecular fibrous hydrogel composite to augment USLS repair in our newly developed animal model. With a carrier hydrogel to encapsulate the guest-host fibers, the material was used to augment the USL-vaginal vault interface created during the USLS procedure. At 24 weeks post-operative, histological analysis demonstrated a reduction in collagen content in both the USLS (51.6 ± 0.7%) and the USLS+H (72.4 ± 2.7%) groups compared to the native control (USL, 87.1 ± 0.7%) showing the impact of the suture repair on the vaginal vault tissue structure. However, the differences in the muscle fiber content (USL: 12.9 ± 0.7%, USLS: 48.4 ± 0.7%, USLS+H: 27.6 ± 2.7%) provide additional context for the mechanical pull-off test and the improved pull-out load of the USLS+H group compared to the USLS suture only group. Applying an in situ tensile testing method, the repair with hydrogel augmentation significantly increased the pull-out load (≈1.4 N) compared to the USLS procedure with sutures alone (≈0.9 N). This demonstrated that the hydrogel assisted in recovery of mechanical properties to be closer to the intact USL tissue (pull-out force ≈1.7 N). In vivo hydrogel degradation tracking demonstrated exponential decay of fluorescent signal resulting in near dissolution of the hydrogel at 6 weeks post-surgery (≈94% degraded), further supporting the premise that superior tissue healing and integration accounts for the recovery of tensile resistance. Together, these results support the potential of this hydrogel platform to augment USLS procedures.

4. Experimental Section

Ad-MeHA and CD-MeHA Hydrogel Synthesis: Hyaluronic acid (HA) was functionalized with photoreactive methacrylates (Me)[89] and then either adamantane (Ad) or β-cyclodextrin (CD)[53] as previously described. Briefly, the HA backbone was methacrylated to produce methacrylate-modified HA (MeHA) via esterification with the primary hydroxyl group of sodium HA at pH 8–9. Next, the MeHA was reacted with proton exchange resin and titrated with tert-butyl ammonium salt (TBA)-OH to yield methacrylated HA-TBA (MeHA-TBA). Ad-modified MeHA (Ad-MeHA) and β-CD-modified MeHA (CD-MeHA) were then synthesized by anhydrous coupling. In Ad-MeHA synthesis, MeHA was modified with 1-adamantane acetic acid via di-tert-butyl bicarbonate (BOC_2O)/4-dimethylaminopyridine (DMAP) esterification. Separately, CD-MeHA was prepared by coupling 6-(6-aminohexyl)amino-6-deoxy-β-cyclodextrin (CD-HDA) to HA via (benzotriazol-1-yloxy) tris(dimethylamino) phosphonium hexafluorophosphate (BOP) amidation. Synthesis products were dialyzed against deionized water, frozen, and lyophilized. The degree of HA modification with Me was controlled by the amount of methacrylic anhydride introduced during synthesis and was determined to be 16%. Modification of the HA backbone with Ad and CD was determined to be 16.5% (Figure S9, Supporting Information) and 16% (Figure S10, Supporting Information) respectively, with all percentages calculated by ^{1}H NMR.

Solid-Phase Peptide Synthesis: Using a Liberty Blue automated microwave-assisted peptide synthesizer, peptides were synthesized via solid-phase synthesis as described previously.[90,91] Briefly, rink Amide MBHA high-loaded (0.78 mmol g^{-1}) resin was used along with solid-supported Fmoc-protected amino acid residues. The resin was swelled with 20% (v/v) piperidine in DMF and the amino acids were sequentially added from C to N-terminus. The resulting peptides were collected and cleaved in 92.5% trifluoroacetic acid, 2.5% triisopropylsilane, 2.5% (2,2-(ethylenedioxy)diethanethiol), and 2.5% water for 2 h and filtered to separate the resin. Two methacrylate-modified peptides were synthesized for use in the hydrogel system: an MMP-degradable peptide (MeP, Methacrylate-GGNS-VPMS↓MRGG-GNCG, Figure S11, Supporting Information) and carrier peptide (Methacrylate-GKKCG) for later fluorophore conjugation. A Cy-7.5 fluorophore (cyanine7.5-maleimide, Lumiprobe) was conjugated to the carrier peptide via thiol-maleimide click chemistry, mixing equal molar amounts in 1x PBS for 2 h. The final product was a Cy7.5 labeled methacrylated peptide (Cy7.5-Me). Peptides were precipitated in cold ether, dried overnight, resuspended in water, frozen, and lyophilized. Synthesis was confirmed via matrix-assisted laser desorption/ionization (MALDI).

MePHA Hydrogel Synthesis: Methacrylated degradable peptide (MeP)-modified HA (MePHA) was synthesized as previously described.[91] Briefly, the HA backbone was modified with maleimide (Ma) groups to facilitate the aqueous addition of the MeP via thiol-maleimide "click" chemistry. In the first step, maleimide HA (MaHA) was synthesized by reacting aminated maleimide salt with tetrabutylammonium-HA (HA-TBA) via a BOP coupling agent to form an amide linkage between the carboxyl group of HA and the amine group of the maleimide salt. The thiolated peptide (containing a cysteine residue) was synthesized with a terminal methacrylate group to allow for later UV light-initiated cross-linking. ^{1}H NMR confirmed 22% maleimide modification of the HA backbone (Figure S12, Supporting Information) followed by successful conjugation with the MeP to produce MePHA (Figure S13, Supporting Information).

Electrospinning: Ad-MeHA and CD-MeHA were dissolved at 2% (w/v) in DI water along with 3.5% (w/v) poly(ethylene oxide) (PEO, 900 kDa) and 0.05% (w/v) Irgacure 2959 (I2959) for 24–48 h prior to electrospinning. The polymer solutions were electrospun (Figure S1A, Supporting Information) using an Elmarco NanoSpider (NS Lab) with the following collection parameters: applied voltage: ≈45 kV, electrode distance: 22 cm, orifice

diameter: 0.7 mm, substrate: Teflon paper, substrate speed: 20 mm min^{-1}, carriage speed: 100 mm s^{-1}. Hydrogel nanofibers were deposited onto Teflon paper, placed into a container which was purged with nitrogen, and cross-linked with UV light (254 nm) for 10 min (VWR Cross-linker Box, 115 V) at 900 J cm^{-2}.

Hydrogel Formulations: This lab had previously described the process of collecting and preparing the guest and host electrospun fibers.[53] Briefly, guest Ad-MeHA and host CD-MeHA fibers were hydrated (0.1% w/v in DI water) overnight at 37 °C to remove PEO from the electrospinning process, centrifuged, supernatant discarded, and then lyophilized. Once dry, the fibers were again hydrated at 0.1% w/v in DI water, allowed to swell at 37 °C for at least 2 h, and then passed through needles of progressively smaller gauge sizes (16G-30G) via trituration. This process separated any adjoined fibers and resulted in a reproducible fiber suspension. MePHA (6 w/v%) was added to envelope the Ad-MeHA/CD-MeHA mixed fibers along with 1 mM lithium acylphosphinate (LAP) to allow for UV light-initiated polymerization (365 nm, 10 mW cm^{-2}). The final formulation resulted in 70 v/v% of fibers and 30 v/v% of the MePHA with LAP solution.

Rheology: All rheological measurements were performed on an Anton Paar MCR 302 rheometer with the plate temperature set at 37 °C as described previously.[53] The hydrogel formulation was tested using a parallel plate (PP08-S; 8 mm diameter, sand blasted) geometry and 25 µm gap distance. Injectability of the hydrogel formulation was tested via a cyclic deformation test alternating between 0.5% and 250% strain to verify shear-thinning and self-healing capabilities. Next, a time sweep (1 Hz, 0.5% strain) with UV cross-linking (365 nm, 10 mW cm^{-2}, 2 min) was performed.

Cytocompatibility and Hemocompatibility Evaluations: Evaluation of cytocompatibility and hemocompatibility ($n = 4$) was conducted using an Alamar blue assay (Invitrogen) with human mesenchymal stromal cells (hMSCs) and via material incubation with rat red blood cells (RBCs), respectively. In vitro testing of the hydrogel cytotoxicity followed ISO 10 993 standards where the hydrogel components were added to cell culture media (1% w/v) and then applied to a monolayer culture of hMSCs and C2C12s. Cells were seeded at 30 000 hMSCs per well and 35 000 C2C12s per well in a 24-well plate with the Alamar blue applied at time intervals of 3 and 5 days of culture. Metabolically active cells reduce the Alamar blue reagent to a fluorescent byproduct (resorufin). Fluorescent signal was read by a plate reader at 565 nm (excitation), 595 nm (emission) after incubation for 4 h in the dark. Hemolysis testing followed ISO 10 993 and ASTM F756 standards where blood was harvested immediately prior to assay preparation. Fresh blood was suspended in 0.01% heparin (Sigma Aldrich) in PBS. The mixture was immediately centrifuged at 1000 rpm for 15 min and then washed with PBS until the supernatant above the pellet of RBCs was clear. The RBCs were then diluted using PBS and incubated for 1 h at 37 °C with the hydrogel components. After incubation, the RBCs were collected and centrifuged again at 1000 rpm for 15 min before the absorbance of the supernatants were read at 540 nm using a plate reader. The results are calculated as hemolysis (%)

$$\text{Hemolysis } (\%) = \frac{OD_t - OD_n}{OD_p - OD_n} \times 100\% \quad (1)$$

where OD_t, OD_n, and OD_p are the absorbance values of the samples, negative control (PBS), and positive control (0.1% Triton X-100), respectively.

Animal Care: This study was conducted in compliance with the Animal Welfare Act, the Implementing Animal Welfare Regulations, and in accordance with the principles of the Guide for the Care and Use of Laboratory Animals. The University of Virginia Animal Care and Use Committee approved all animal procedures. A total of 30 multiparous (2 litter) female Lewis rat breeders (Charles River Laboratories) weighing 274.8 ± 19.3 g were pair housed in a vivarium accredited by the American Association for the Accreditation of Laboratory Animal Care and provided with food and water ad libitum. Animals were between 4 and 6 months of age to accommodate the 2 litter requirement. Animals were maintained on a 12 h light-dark cycle. A total of $n = 10$ animals were used in this study per group, with $n = 8$ used for mechanical testing and $n = 2$ for histological tissue collection.

Anesthesia, Pain Management, and Antibiotics: All animal-related details were described in detail previously.[36] Briefly, animals were anesthetized via isoflurane and the surgical site was aseptically prepared by repeated washes with alcohol and iodine. The depth of anesthesia was monitored by the response of the animal to a slight toe pinch, where the lack of response was considered the surgical plane of anesthesia. Core temperature was maintained using a heated water perfusion system. Rats were administered slow-release buprenorphine (Bup XR – 72 h; 1.3 mg kg^{-1}, subcutaneously), slow-release meloxicam (72 h; 1.0 mg kg^{-1}, subcutaneously), and baytril (10 mg kg^{-1}, subcutaneously) prior to surgery. Since meloxicam is known to cause dehydration, rats were also administered 0.9% sterile saline (10 mL kg^{-1}, subcutaneously). Animal pain and distress were monitored daily by qualified members of the veterinary staff to determine the need for additional analgesia.

Surgical Procedures: Using aseptic technique, a vertical midline skin incision was made along the abdomen and the fascia was separated to expose the underlying abdominal cavity. Hysterectomy was performed, where the uterine horns were trimmed after separation from the ovaries and fat pads, leaving the cervix, vagina, and its support tissues intact. One delayed absorbable suture (3-0 polydioxanone, PDS II, Ethicon) was placed through the vaginal vault and the exposed uterosacral ligament (USL) bilaterally. The PDS suture material was chosen because it is the type most used often used in clinical practice for USLS surgeries. It was a delayed absorbable suture that had a slower degradation rate compared to other sutures such as Vicryl. PDS had been showed to be equally successful compared to permanent suture in humans,[92] making it a clinically reasonable choice in humans as well as in the rat model. Tying the sutures down simultaneously closed the vaginal vault and elevated it toward the USLs. A single uterosacral stitch was used due to limited space along the USL in the rat model and the goal to had spatial ability to perform mechanical testing of the ligament. For hydrogel augmentation, material components were sterilized separately and then prepared aseptically. A total of 40 µL (20 µL each side) hydrogel precursor was delivered over the sutures and then UV cross-linked (365 nm, 10 mW cm^{-2}, 2 min). Animals in the sham experimental group were used for healthy animal controls to assess normal tissue properties. Animals were randomly assigned to one of the following experimental groups: sham surgery with no prolapse repair (USL; $n = 8$), prolapse repair (USLS; $n = 8$), or prolapse hydrogel repair (USLS+H; $n = 8$).

In Vivo Hydrogel Degradation Analysis: To evaluate in vivo hydrogel degradation, hydrogel nanofibers were labeled with the Cy7.5-Me peptide via UV light-initiated conjugation in the presence of LAP photoinitiator. The fluorophore was covalently bound via the methacrylates present on the surface of the hydrogel fibers during photocuring. Serial images were taken during a 6 week period postoperative using a LagoX live imaging system (excitation: 770 nm, emission: 810 nm) with signal intensity measured by integrating equivalent areas over the region of interest. Quantified signal was normalized to peak intensity for individual hydrogel boluses immediately following surgery and then averaged to obtain degradation profiles for each hydrogel ($n = 4$). Signal decay was fit with an exponential one-phase decay line using GraphPad Prism.

Mechanical Testing of the USLS and Prolapse Repair Junction: At 24 weeks post-surgery, the uterosacral ligament (USL) or USLS prolapse repair junction (USLS, USLS+H) were prepared for mechanical testing using a single column Instron (5943 S3873) universal testing system. A 10 N load cell was used for testing. Methods were described, including a video demonstration, in previous work.[36] Briefly, umbilical tape (Ethicon U10T) was threaded beneath the suture/new tissue formation between the vaginal vault and the uterosacral ligament. The tissue was pre-loaded at 0.015 N and then preconditioned at an elongation rate of 0.1 mm s^{-1} for 1 min. The tissue was then pulled to failure at the same elongation rate.

Histological Preparation, Imaging, and Analysis: Histological studies were conducted on $n = 2$ animals per group. Slides from each animal were stained with Masson's trichrome (MT) and hematoxylin and eosin (H&E). Following tissue retrieval, orientation was conserved by pinning tissue to a clear rubber holder followed by fixation in 10% formalin at 4 °C. Processing, embedding of rat reproductive structures in paraffin wax, and staining

were conducted by the Research Histology Core at the University of Virginia School of Medicine. Serial cross sections measuring 5 µm thick were cut prior to staining with either H&E or MT. Whole longitudinal section tile scan images were acquired using a light microscope (Leica Thunder Imager with Leica Application Suite X software). Vaginal vault areas of interest tile scan images were acquired at 40x magnification. Muscle (*red*) and collagen (*blue*) content were determined from the MT-stained slides. Five areas, 1500×1500 pixels, were randomly selected from 40x MT images for color quantification analysis. Using ImageJ software (NIH), blue and red pixels were identified using the "RGB Measure" plugin tool. Total red and blue pixel count values were used to create percentage blue and red counts for each image. Final reported values were averaged over the five imaged areas selected from a given histological slide, over the total number of slides, and finally over the total number of animals.

Statistical Analysis: All data were presented as means and standard deviation or standard error of mean (SEM). The data were statistically analyzed by one-way ANOVA followed by Tukey-Kramer multiple comparisons testing using GraphPad Prism 9.0. *ns* represents no statistically significant differences. P values < 0.05 were considered statistically significant where $*P < 0.05$, $**P < 0.01$, $***P < 0.001$ and $****P < 0.0001$.

Supporting Information

Supporting Information is available from the Wiley Online Library or from the author.

Acknowledgements

The authors thank Luna Innovations for the use of their NanoSpider for hydrogel nanofiber production, Prof. Rachel Letteri for the use of her peptide synthesizer, and Prof. George Christ for use of his surgical space. This work was supported by the UVA-Coulter Translational Research Partnership and the DoD (W81XWH-19-1-0157).

Conflict of Interest

The authors declare no conflict of interest.

Data Availability Statement

The data that support the findings of this study are available from the corresponding author upon reasonable request.

Keywords

hydrogels, nanofibers, pelvic organ prolapse, tissue engineering, uterosacral ligaments

Received: January 8, 2023
Revised: May 11, 2023
Published online: May 31, 2023

[1] E. C. Samuelsson, F. T. A. Victor, G. Tibblin, K. F. Svardsudd, *Am. J. Obstet. Gynecol.* **1999**, *180*, 299.
[2] B. T. Haylen, C. F. Maher, M. D. Barber, S. Camargo, V. Dandolu, A. Digesu, H. B. Goldman, M. Huser, A. L. Milani, P. A. Moran, G. N. Schaer, M. I. J. Withagen, *Neurourol. Urodyn.* **2016**, *35*, 137.
[3] S. Herschorn, *Rev. Urol.* **2004**, *6*, S2.
[4] J. E. Jelovsek, C. Maher, M. D. Barber, *Lancet* **2007**, *369*, 1027.
[5] Urogynecologic Surgical Mesh: Update on the Safety and Effectiveness of Transvaginal Placement for Pelvic Organ Prolapse, https://www.fda.gov/media/81123/download (accessed: July **2011**).
[6] FDA takes action to protect women's health, orders manufacturers of surgical mesh intended for transvaginal repair of pelvic organ prolapse to stop selling all devices, https://www.fda.gov/news-events/press-announcements/fda-takes-action-protect-womens-health-orders-manufacturers-surgical-mesh-intended-transvaginal (accessed: April **2019**).
[7] M. Aubé, L. M. Tu, *Women's Health (Lond. Engl)*. **2018**, *14*, 1745506518776498.
[8] R. S. Lavelle, A. L. Christie, F. Alhalabi, P. E. Zimmern, *J. Urol.* **2016**, *195*, 1014.
[9] J. E. Jelovsek, M. D. Barber, P. Norton, L. Brubaker, M. Gantz, H. E. Richter, A. Weidner, S. Menefee, J. Schaffer, N. Pugh, S. Meikle, *JAMA – J. Am. Med. Assoc.* **2018**, *319*, 1554.
[10] A. A. Mirin, *J. Women's Health* **2021**, *30*, 956.
[11] M. J. Grimm, *Interface Focus* **2019**, *9*, 20190017.
[12] History of women's participation in clinical research, https://orwh.od.nih.gov/toolkit/recruitment/history (accessed: January 2023).
[13] A. Shikanov, M. Xu, T. K. Woodruff, L. D. Shea, *Biomaterials* **2009**, *30*, 5476.
[14] Y. Chen, S. Chen, K. Ok, F. E. Duncan, T. V. O'Halloran, T. K. Woodruff, *J. Biol. Chem.* **2022**, *299*, 102731.
[15] J. S. Gnecco, A. T. Brown, E. L. Kan, L. Baugh, C. Ives, M. Loring, L. G. Griffith, *Semin. Reprod. Med.* **2020**, *38*, 179.
[16] C. J. Cook, A. E. Miller, T. H. Barker, Y. Di, K. C. Fogg, *Matrix Biol. Plus* **2022**, *15*, 100117.
[17] A. R. Murphy, H. Campo, J. J. Kim, *Nat. Rev. Endocrinol.* **2022**, *18*, 727.
[18] J. Robinson, A. Shikanov, B. Harley, *Tissue Eng. Part A* **2020**, *26*, 685.
[19] R. De Vita, J. Munson, *Ann. Biomed. Eng.* **2021**, *49*, 1785.
[20] K. S. Miller, K. Myers, M. Oyen, *Interface Focus* **2019**, *9*, 20190017.
[21] K. Fogg, N.-H. Tseng, S. R. Peyton, P. Holeman, S. McLoughlin, J. P. Fisher, A. Sutton, A. Shikanov, N. N. Hashemi, Y. Zhang, M. D. House, B. J. Vogt, B. A. Aguado, J. C. Bradford, J. L. Robinson, P. K. Thomas, A. G. Lau, M. L. Oyen, *J. Phys. Mater.* **2022**, *6*, 012501.
[22] I. Cadena, A. Chen, A. Arvidson, K. C. Fogg, *Biomater. Sci.* **2020**, *9*, 1117.
[23] K. L. Swingle, A. S. Ricciardi, W. H. Peranteau, M. J. Mitchell, *Nat. Rev. Bioeng.* **2023**.
[24] J. M. Wu, C. A. Matthews, M. M. Conover, V. Pate, M. J. Funk, *Obstet. Gynecol.* **2014**, *123*, 1201.
[25] P. K. Thompson, R. J. McCrery, E. C. Lotze, H. Sangi-Haghpeykar, *J. Pelvic Med. Surg.* **2008**, *14*, 15.
[26] S. T. Bowen, P. A. Moalli, S. D. Abramowitch, M. E. Lockhart, A. C. Weidner, C. A. Ferrando, C. W. Nager, H. E. Richter, C. R. Rardin, Y. M. Komesu, H. S. Harvie, D. Mazloomdoost, A. Sridhar, M. G. Gantz, *Am. J. Obstet. Gynecol.* **2021**, *225*, 506.e1.
[27] J. M. Wu, A. Kawasaki, A. F. Hundley, A. A. Dieter, E. R. Myers, V. W. Sung, *Am. J. Obstet. Gynecol.* **2011**, *205*, 230.e1.
[28] G. Gigliobianco, S. R. Regueros, N. I. Osman, J. Bissoli, A. J. Bullock, C. R. Chapple, S. MacNeil, *Biomed Res. Int.* **2015**, *2015*, 968087.
[29] X. Wu, Y. Y. Jia, X. Sun, J. Wang, *Eng. Life Sci.* **2020**, *20*, 275.
[30] R. Liang, K. Knight, D. Easley, S. Palcsey, S. Abramowitch, P. A. Moalli, *Acta Biomater.* **2017**, *57*, 324.
[31] K. Christman, M. Alperin, P. Duran, Extracellular Matrix for Treating Pelvic Floor Disorders and Skeletal Muscle Degeneration, US 2022/0296776 A1, **2022**.
[32] S. Mukherjee, S. Darzi, K. Paul, J. A. Werkmeister, C. E. Gargett, *Interface Focus* **2019**, *9*, 20180089.
[33] C. E. Gargett, S. Gurung, S. Darzi, J. A. Werkmeister, S. Mukherjee, *Curr. Opin. Urol.* **2019**, *29*, 450.

[34] H. G. Krause, J. T. Goh, *Curr. Opin. Obstet. Gynecol.* **2009**, *21*, 419.
[35] B. M. Couri, A. T. Lenis, A. Borazjani, M. F. R. Paraiso, M. S. Damaser, *Expert Rev. Obstet. Gynecol.* **2012**, *7*, 249.
[36] B. J. Miller, B. K. Jones, J. S. Turner, S. R. Caliari, M. H. Vaughan, *J. Visualized Exp.* **2022**, *186*, 64311.
[37] S. G. Hansen, M. B. Taskin, M. Chen, L. Wogensen, J. Vinge Nygaard, S. M. Axelsen, *J. Biomed. Mater. Res., Part B* **2019**, *108*, 48.
[38] Y. Wang, Z. Cao, R. Cheng, M. Qin, D. Zhang, L. Deng, X. Chen, W. Cui, *Appl. Mater. Today* **2019**, *15*, 570.
[39] C. R. Chapple, N. I. Osman, A. Mangera, C. Hillary, S. Roman, A. Bullock, S. Macneil, *LUTS: Lower Urinary Tract Symptoms* **2015**, *7*, 63.
[40] K. Paul, S. Darzi, J. A. Werkmeister, C. E. Gargett, S. Mukherjee, *Nanomaterials* **2020**, *10*, 1120.
[41] K. Paul, S. Darzi, G. McPhee, M. P. Del Borgo, J. A. Werkmeister, C. E. Gargett, S. Mukherjee, *Acta Biomater.* **2019**, *97*, 162.
[42] L. Hympanova, M. G. M. C. Mori da Cunha, R. Rynkevic, M. Zündel, M. R. Gallego, J. Vange, G. Callewaert, I. Urbankova, F. Van der Aa, E. Mazza, J. Deprest, *J. Mech. Behav. Biomed. Mater.* **2017**, *74*, 349.
[43] U. Klinge, B. Klosterhalfen, J. Conze, W. Limberg, B. Obolenski, A. P. Öttinger, V. Schumpelick, *Eur. J .Surg.* **1998**, *164*, 951.
[44] F. S. Ayubi, P. J. Armstrong, M. S. Mattia, D. M. Parker, *Hernia* **2008**, *12*, 373.
[45] M. Yuan, M. Hu, F. Dai, Y. Fan, Z. Deng, H. Deng, Y. Cheng, *Mater. Des.* **2021**, *209*, 109984.
[46] J. Whooley, E. M. Cunnane, R. Do Amaral, M. Joyce, E. MacCraith, H. D. Flood, F. J. O'Brien, N. F. Davis, *Tissue Eng., Part B* **2020**, *26*, 475.
[47] M. Vashaghian, S. J. Zaat, T. H. Smit, J. P. Roovers, *Neurourol. Urodyn.* **2018**, *37*, 566.
[48] A. Feola, S. Abramowitch, Z. Jallah, S. Stein, W. Barone, S. Palcsey, P. Moalli, *BJOG* **2013**, *120*, 224.
[49] T.-M. De Witte, L. E. Fratila-Apachitei, A. A. Zadpoor, N. A. Peppas, *Regen. Biomater.* **2018**, *5*, 197.
[50] C. H. Lee, H. J. Shin, I. H. Cho, Y. M. Kang, I. A. Kim, K. D. Park, J. W. Shin, *Biomaterials* **2005**, *26*, 1261.
[51] J. J. Tomasek, G. Gabbiani, B. Hinz, C. Chaponnier, R. A. Brown, *Nat. Rev. Mol. Cell Biol.* **2002**, *3*, 349.
[52] Y. Chang, X. Sun, Q. Li, X. Ding, H. Liu, J. Wang, *Microsc. Res. Tech* **2017**, *80*, 291.
[53] B. Miller, A. Hansrisuk, C. B. Highley, S. R. Caliari, *ACS Biomater. Sci. Eng.* **2021**, *7*, 4164.
[54] R. Iwanaga, D. J. Orlicky, J. Arnett, M. K. Guess, K. J. Hurt, K. A. Connell, *Int. Urogynecol. J.* **2016**, *27*, 1697.
[55] A. N. Gent, S. Kaang, *J. Appl. Polym. Sci.* **1986**, *32*, 4689.
[56] C. D. Spicer, *Polym. Chem.* **2020**, *11*, 184.
[57] J. L. Drury, D. J. Mooney, *Biomaterials* **2003**, *24*, 4337.
[58] S. R. Caliari, J. A. Burdick, *Nat. Methods* **2016**, *13*, 405.
[59] R. Liang, W. Zong, S. Palcsey, S. Abramowitch, P. A. Moalli, *Am. J. Obstet. Gynecol.* **2015**, *212*, 174.e1.
[60] C. B. Highley, G. D. Prestwich, J. A. Burdick, *Curr. Opin. Biotechnol.* **2016**, *40*, 35.
[61] B. M. Baker, B. Trappmann, W. Y. Wang, M. S. Sakar, I. L. Kim, V. B. Shenoy, J. A. Burdick, C. S. Chen, *Nat. Mater.* **2015**, *14*, 1262.
[62] I. Jun, H. S. Han, J. R. Edwards, H. Jeon, *Int. J. Mol. Sci.* **2018**, *19*, 745.
[63] Y. Ji, K. Ghosh, X. Z. Shu, B. Li, J. C. Sokolov, G. D. Prestwich, R. A. F. Clark, M. H. Rafailovich, *Biomaterials* **2006**, *27*, 3782.
[64] E. Peña, B. Calvo, M. A. Martínez, P. Martins, T. Mascarenhas, R. M. N. Jorge, A. Ferreira, M. Doblaré, *Biomech. Model. Mechanobiol.* **2010**, *9*, 35.
[65] P. Martins, A. Lopes Silva-Filho, A. M. Rodrigues Maciel Da Fonseca, A. Santos, L. Santos, T. Mascarenhas, R. M. Natal Jorge, A. J. M. Ferreira, *Gynecol. Obstet. Invest.* **2013**, *75*, 85.
[66] J. L. Lowder, K. Debes, D. K. Moon, N. Howden, S. D. Abramowitch, P. A. Moalli, *Obstet. Gynecol.* **2007**, *109*, 136.
[67] P. A. Moalli, N. S. Howden, J. L. Lowder, J. Navarro, K. M. Debes, S. D. Abramowitch, S. L. Y. Woo, *Am. J. Obstet. Gynecol.* **2005**, *192*, 80.
[68] E. Hui, K. I. Gimeno, G. Guan, S. R. Caliari, *Biomacromolecules* **2019**, *20*, 4126.
[69] M. C. Bélanger, Y. Marois, *J. Biomed. Mater. Res.* **2001**, *58*, 467.
[70] J. A. Bickhaus, M. O. Fraser, A. C. Weidner, F. L. Jayes, C. L. Amundsen, K. Gall, A. T. Miller, F. C. Marini, S. J. Robboy, N. Y. Siddiqui, *Female Pelvic Med. Reconstr. Surg.* **2021**, *27*, 469.
[71] I. M. Basurto, J. A. Passipieri, G. M. Gardner, K. K. Smith, A. R. Amacher, A. I. Hansrisuk, G. J. Christ, S. R. Caliari, *Tissue Eng., Part A* **2022**, *28*, 312.
[72] K. A. Kyburz, K. S. Anseth, *Ann. Biomed. Eng.* **2015**, *43*, 489.
[73] M. W. Tibbitt, K. S. Anseth, *Biotechnol. Bioeng.* **2009**, *103*, 655.
[74] T. Molloy, Y. Wang, G. A. C. Murrell, *Sport. Med.* **2003**, *33*, 381.
[75] O. Shynlova, M. A. T. Bortolini, M. Alarab, *Int. Braz. J. Urol.* **2013**, *39*, 257.
[76] E. V. Vodegel, A. W. Kastelein, C. H. J. R. Jansen, J. Limpens, S. E. Zwolsman, J. P. W. R. Roovers, C. R. Hooijmans, Z. Guler, *Neurourol. Urodyn.* **2022**, *41*, 115.
[77] A. Feola, P. Moalli, M. Alperin, R. Duerr, R. E. Gandley, S. Abramowitch, *Ann. Biomed. Eng.* **2011**, *39*, 549.
[78] S. Abramowitch, D. Easley, in *Biomech. Female Pelvic Floor*, (Eds: L. Hoyte, M. Damaser), Academic Press, Cambridge **2016**, pp. 109.
[79] K. Donaldson, R. De Vita, *Ann. Biomed. Eng.* **2023**, *51*, 702.
[80] E. N. de Carvalho Calvi, F. X. Nahas, M. V. Barbosa, J. A. Calil, S. S. M. Ihara, M. de Souza Silva, M. F. de Franco, L. M. Ferreira, *Acta Cir. Bras.* **2012**, *27*, 681.
[81] A. Baah-Dwomoh, M. Alperin, M. Cook, R. De Vita, *Ann. Biomed. Eng.* **2018**, *46*, 2036.
[82] C. C. Takano, M. J. B. C. Girão, M. G. F. Sartori, R. A. Castro, R. M. Arruda, M. J. Simões, E. C. Baracat, G. Rodrigues de Lima, *Int. Urogynecol. J.* **2002**, *13*, 342.
[83] R. Gong, Z. Xia, *Eur. J. Obstet. Gynecol. Reprod. Biol.* **2019**, *234*, 185.
[84] S. F. Badylak, D. O. Freytes, T. W. Gilbert, *Acta Biomater.* **2009**, *5*, 1.
[85] K. Kenton, E. R. Mueller, *BJU Int.* **2006**, *98*, 6.
[86] R. Palmerola, N. Rosenblum, *Curr. Urol. Rep.* **2019**, *20*, 70.
[87] A. L. Olsen, V. J. Smith, J. O. Bergstrom, J. C. Colling, A. L. Clark, *Obstet. Gynecol.* **1997**, *89*, 501.
[88] N. Y. Siddiqui, C. L. Grimes, E. R. Casiano, H. T. Abed, P. C. Jeppson, C. K. Olivera, T. V. Sanses, A. C. Steinberg, M. M. South, E. M. Balk, V. W. Sung, *Obstet. Gynecol.* **2015**, *125*, 44.
[89] H. G. Sundararaghavan, J. A. Burdick, *Biomacromolecules* **2011**, *12*, 2344.
[90] J. Patterson, J. A. Hubbell, *Biomaterials* **2010**, *31*, 7836.
[91] R. J. Wade, E. J. Bassin, C. B. Rodell, J. A. Burdick, *Nat. Commun.* **2015**, *6*, 6639.
[92] B. L. Pollack, P. Popiel, M. C. Toaff, E. Drugge, A. Bielawski, A. Sacks, M. Bibi, R. Friedman-Ciment, K. Lebron, L. Alishahian, D. Phillips, S. R. Rubino, S. Pollack, R. S. Khan, E. S. Khan, D. M. Pape, C. L. Grimes, *Obstet Gynecol* **2023**, *141*, 268.